PROCEEDINGS, 51st Workshop on Geothermal Reservoir Engineering
Stanford University, Stanford, California, February 9-11, 2026
SGP-TR-230

Integration of Maximum Magnitude Forecast and Ground Motion Prediction for Real-Time Seismic Hazard Assessment at Utah FORGE

Xiaoming Zhang[1], Noam Zach Dvory[1,2]

[1]Energy and Geoscience Institute, the University of Utah, Salt Lake City, UT, USA

[2]Department of Civil and Environmental Engineering, the University of Utah, Salt Lake City, UT, USA

Xiaoming.Zhang@utah.edu

nzd@egi.utah.edu

Keywords: Enhanced Geothermal Systems (EGS), Maximum Magnitude M_{max} Prediction, Ground Motion Prediction, Seismic Hazard Assessment

ABSTRACT

Accurate ground motion prediction is essential for assessing the potential impact of induced seismicity during fluid injection in enhanced geothermal systems (EGS). Building on our maximum magnitude (M_{max}) forecasting framework, we integrated M_{max} predictions with ground-motion prediction equations (GMPEs) to evaluate spatial and temporal variations in seismic hazard at the Utah FORGE site. The approach combined the predicted M_{max} values with GMPEs that account for local geological and site effects, including shallow time-averaged shear-wave velocity (Vs30) and epicentral distance. By dynamically linking source-level forecasts to site-level motion estimates, the model provided updated predictions of Peak Ground Acceleration (PGA) and Peak Ground Velocity (PGV) at nearby population centers and infrastructure nodes. Preliminary results from the 2022 and 2024 FORGE stimulations indicated that incorporating evolving M_{max} forecasts improved the reliability of PGA and PGV estimates under changing injection and post-injection conditions. This integrated framework provides a pathway to real-time, data-informed seismic hazard assessment in EGS operations, enhancing risk mitigation and supporting the refinement of traffic-light protocols.

1. INTRODUCTION

Induced seismicity associated with fluid injection poses a key operational and societal challenge for enhanced geothermal systems (EGS) (Majer et al., 2007; Niemz et al., 2024; Zhang et al., 2025; Zhang, Shimony, Song, et al., 2026; Zhang, Shimony, Wygodny, et al., 2026; Zhang & Dvory, 2025). While most induced events are small, occasional larger-magnitude earthquakes can produce ground motions felt at the surface, raising concerns for infrastructure integrity, public safety, and regulatory compliance (Ellsworth, 2013; Ellsworth et al., 2019). Consequently, reliable real-time seismic hazard assessment is a central component of EGS risk management and traffic light protocol (TLP) implementation (Schultz et al., 2021).

Traditional seismic hazard assessments often rely on static assumptions regarding maximum credible magnitude and ground motion levels. However, injection-induced seismicity is inherently nonstationary, with seismicity rates, stress conditions, and maximum magnitude evolving in response to operational changes. Recent studies have demonstrated that the maximum magnitude (M_{max}) of induced earthquakes can be forecast dynamically based on injection history, cumulative seismic moment release, and geomechanical constraints (van der Elst et al., 2016; Gutenberg & Richter, 1944; Hallo et al., 2014; Li et al., 2022; Shapiro et al., 2010). While such forecasts provide critical source-level information, their direct implications for ground shaking and surface impacts are not always explicit.

Ground motion prediction equations (GMPEs) (Atkinson, 2015; Atkinson & Boore, 2006; Bommer et al., 2010; Mahani & Kao, 2017) provide a well-established framework for translating earthquake source parameters into site-specific shaking intensity measures, such as Peak Ground Acceleration (PGA) and Peak Ground Velocity (PGV). When combined with predicted M_{max} induced by FORGE stimulation activities, GMPEs enable estimation of upper-bound PGA and PGV levels, which are key parameters for evaluating both damage potential and nuisance impacts. The relationship between M_{max} and damage or nuisance effects can be quantified using ground motion–based nuisance functions (Schultz et al., 2021) and structural fragility functions (Chase et al., 2019). In general, larger M_{max} values are associated with stronger ground motions and increased potential impacts on the ground surface, infrastructure, and nearby populations. Accurate forecasting of M_{max} is therefore critical, as ground motion predictions conditioned on M_{max} provide actionable information on the expected levels of PGA and PGV associated with evolving seismic hazard.

In this study, we focused on M_{max} prediction as a key input to ground motion estimation at the Utah FORGE site. Using seismic and operational data from the 2022 and 2024 stimulation activities (Dyer, 2022; Dyer et al., 2024; England, 2024; McLennan, 2022), we evaluate how evolving M_{max} estimates translate into spatially variable PGA and PGV levels at selected surface locations. The results demonstrate that changes in M_{max} directly and measurably affect predicted ground motions. Moreover, explicitly accounting for uncertainties in both M_{max} forecasting and GMPE-based ground-motion prediction enhances the robustness and reliability of real-time seismic hazard assessments during EGS operations.

2. STUDY SITE

2.1 Utah FORGE

The Utah Frontier Observatory for Research in Geothermal Energy (FORGE) is a dedicated EGS research site located in Milford, Utah. The site targets crystalline basement rocks at depths of approximately 2–3 km and has hosted multiple hydraulic stimulation experiments to enhance reservoir permeability. Comprehensive seismic monitoring is a cornerstone of FORGE operations, providing a high-quality dataset for studying induced seismicity and hazard. The seismic monitoring network at Utah FORGE includes downhole geophones, surface seismometers, and distributed acoustic sensing (DAS) systems (Dyer, 2022; Dyer et al., 2024). For this study, we used earthquake catalogs derived from the 2022 and 2024 stimulation activities. These catalogs served as inputs for predicting $M_{max,}$ which was used in the subsequent hazard analysis.

2.2 Site Data

2.1.1 Depth of Events

The depth of hydraulic fracturing at the Utah site is around 3 km, with perturbations shown in Figure 1. The depth model consisted of a uniform base depth of 3 km with superimposed spatially random perturbations uniformly distributed within ±0.2 km, producing a heterogeneous depth field ranging from 2.8 to 3.2 km.

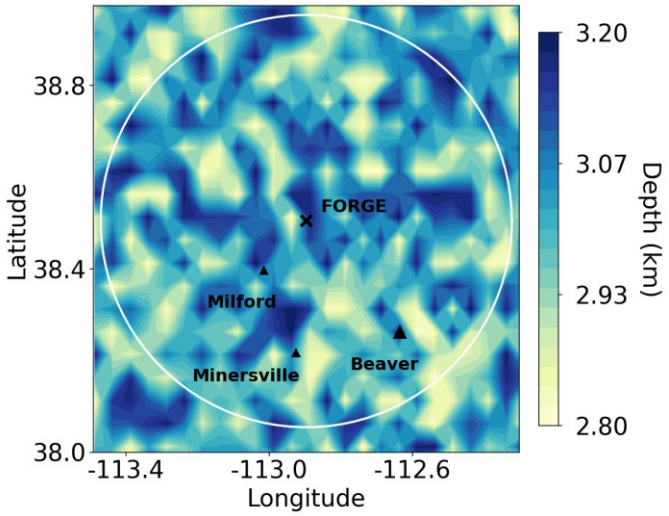

Figure 1: Spatial distribution of earthquake source depths across the Utah FORGE region.

2.1.2 Site amplification

Near-surface velocity structure and local geology can significantly influence earthquake ground motions by either amplifying or attenuating seismic waves. The parameter Vs30, defined as the time-averaged shear-wave velocity in the upper 30 m of the subsurface (Castellaro et al., 2008), is commonly used to characterize site amplification effects. In this study, Vs30 was modeled as a linear horizontal gradient ranging from 250 to 300 m/s, superimposed with lognormal random variability (log-space standard deviation of 0.1) to represent spatial heterogeneity, as shown in Figure 2.

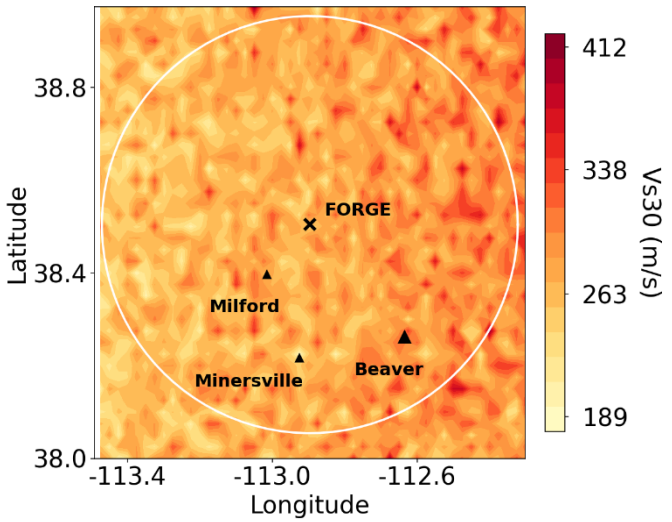

Figure 2: Vs30 model used to represent site amplification effects across the Utah FORGE region.

2.1.3 Population

A gridded household exposure model was constructed for the Utah FORGE region using town-specific population densities scaled by grid cell area. Rural areas were assigned a household density of 0, while Minersville (807), Milford (1,431), and Beaver (3,592) were represented using polygon-based population assignments. The resulting population map provided a spatially explicit representation of household exposure for risk assessment, as shown in Figure 3.

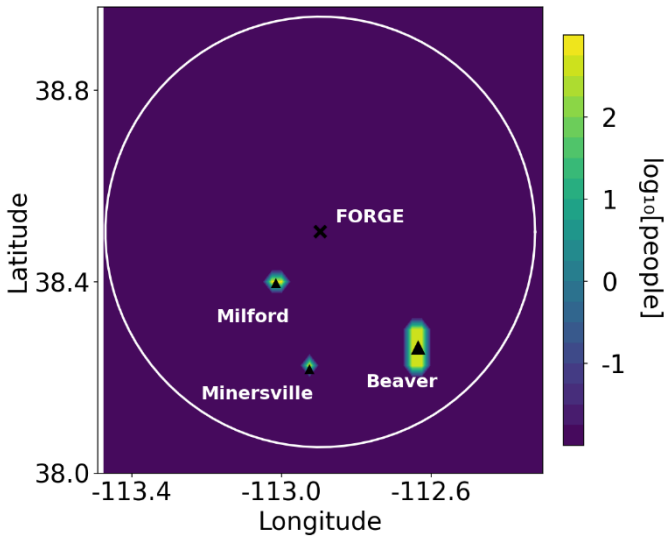

Figure 3: Gridded household exposure map for the Utah FORGE region.

3. METHODOLOGY

3.1 Maximum Magnitude Prediction

McGarr (2014) found that the maximum magnitude of earthquakes induced by fluid injection is generally limited by the total injected fluid volume, with the maximum seismic moment estimated as the product of the injected fluid volume and the shear modulus. This volume-based upper bound was supported by case studies and offers a practical, though not absolute, constraint on the largest expected induced earthquakes during injection operations. The estimated upper-bound moment magnitude is expressed as:

$$M_{max} = \frac{2}{3} log_{10}[G\Delta V(t)] - 6.033 \quad (1)$$

where G is the shear modulus, and ΔV is the cumulative injected fluid volume.

To account for aseismic slip, Hallo et al. (Hallo et al., 2012, 2014) proposed a modification to Eq. (1) by introducing the concept of a seismic efficiency ratio (S_{EFR}), defined as the ratio of the observed cumulative scalar seismic moment to the theoretical cumulative moment. This ratio estimates the portion of the seismic deformation to the total deformation, and is expressed as:

$$S_{EFR} = \frac{\sum M_0}{G\Delta V} \tag{2}$$

where $\sum M_0$ is the cumulative seismic moment of the observed period. With the introduction of S_{EFR}, M_{max} can be defined as:

$$M_{max} = \frac{2}{3} log_{10}[S_{EFR} G \Delta V(t)] - 6.033 \tag{3}$$

The two methods provide estimates of M_{max} that are directly incorporated into subsequent ground motion predictions.

3.2 Ground Motion Prediction

Ground motions associated with induced seismicity are a key factor in evaluating both nuisance and potential damage impacts during EGS operations. To translate source-level earthquake characteristics into site-specific shaking intensity measures, we utilized the Atkinson GMPE (Atkinson, 2015), which has been shown to perform well for small-to-moderate magnitude earthquakes and short source–receiver distances typical of geothermal and hydraulic stimulation settings. The peak ground motion Y (either PGV in cm/s or PGA cm/s^2) is calculated in $\log_{10}$ space as follows:

$$log_{10}(Y) = (c_0 + \Delta c_0) + c_1 M + c_2 M^2 + c_3 log_{10}(R) + \Delta c_{dist} + F_s + \epsilon \cdot dE \tag{4}$$

where M is the moment magnitude, R is the effective distance (km), Δc_{dist} is the distance adjustment for mid-to-long ranges, F_s is the site amplification factor, $\epsilon \cdot dE$ and is the uncertainty term.

3.3 Integration of M_{max} and GMPEs

The integrated hazard framework directly links estimated M_{max} values to ground-motion predictions to quantify the potential surface shaking associated with induced seismicity. Within this framework, M_{max} was treated as a scenario source magnitude that represents the upper bound of the expected earthquake size during stimulation operations. For each M_{max} scenario, the corresponding PGA and PGV values were computed at selected surface locations using the adopted ground-motion prediction equations.

The resulting PGA and PGV estimates can provide a physically interpretable way of evaluating the accuracy of the predicted M_{max}. Specifically, larger M_{max} values lead to higher predicted ground motions, which may reach or exceed human perception thresholds. In cases where predicted ground motions imply perceptible shaking, but no such observations are reported at nearby population centers, the associated M_{max} scenario may be considered overly conservative. The comparison between predicted ground motions and the perceived shaking level provides a validation for M_{max} estimates. In this way, ground motion predictions serve not only as a measure of potential hazard but also as an indirect validation tool for assessing whether predicted M_{max} values are reasonable within the operational context.

4. RESULTS

4.1 M_{max} prediction

The M_{max} prediction was evaluated using Eq. (1) (McGarr's model) and Eq. (3) (Hallo's model), both of which relate induced seismicity to injection-related parameters but rely on different physical assumptions. Figures 4 and 5 show the temporal evolution of observed M_w together with the predicted M_{max} values for the April 2022 and April 2024 Utah FORGE stimulations, respectively. In both cases, McGarr's model predicted a rapid increase in M_{max} early in the injection process, reaching values that substantially exceed the largest observed magnitudes. This behavior reflects the conservative nature of the volume-based formulation and its sensitivity to increases in cumulative injected volume.

Hallo's model produced lower M_{max} estimates, closely tracking the evolution of cumulative seismic moment. For the April 2022 stimulation (Figure 4), the predicted M_{max} from Hallo's model slightly exceeds the observed maximum magnitude, while remaining well below the McGarr-based estimate. A similar pattern is observed for the April 2024 stimulation (Figure 5), where Hallo's predicted M_{max} closely aligns with the upper range of observed seismicity and exhibits limited growth after the main injection phases.

Overall, the comparison shows that McGarr's model provides a conservative upper bound on M_{max}, whereas Hallo's model yields the predictions that are more consistent with the observed magnitude distribution at Utah FORGE. These differences motivate the use of both models in subsequent ground-motion analyses, allowing the assessment of operational risk under both conservative and observation-constrained M_{max} scenarios.

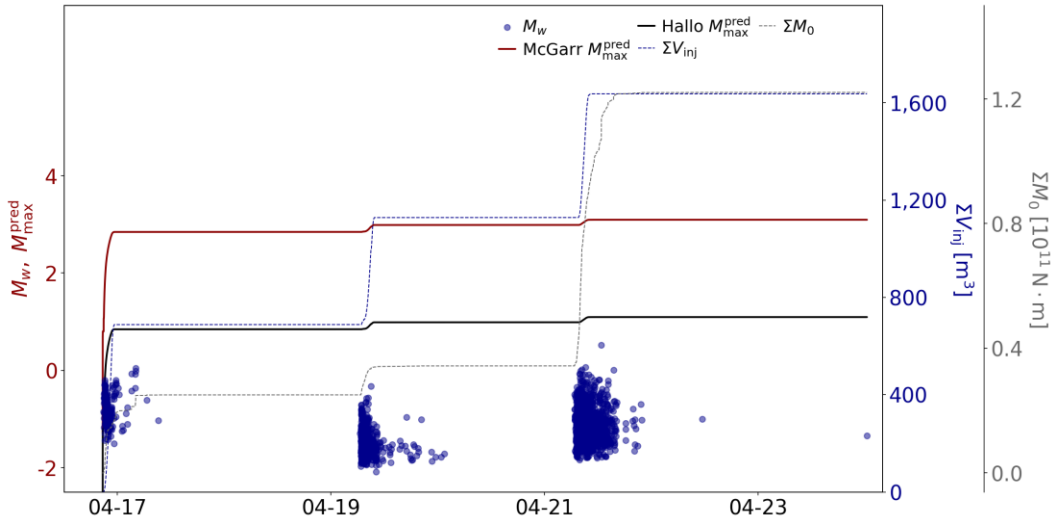

Figure 4: Temporal evolution of observed M_w and predicted M_{max} during the April 2022 Utah FORGE stimulation. Predictions are shown for McGarr's model and Hallo's model, together with cumulative injected volume and cumulative seismic moment.

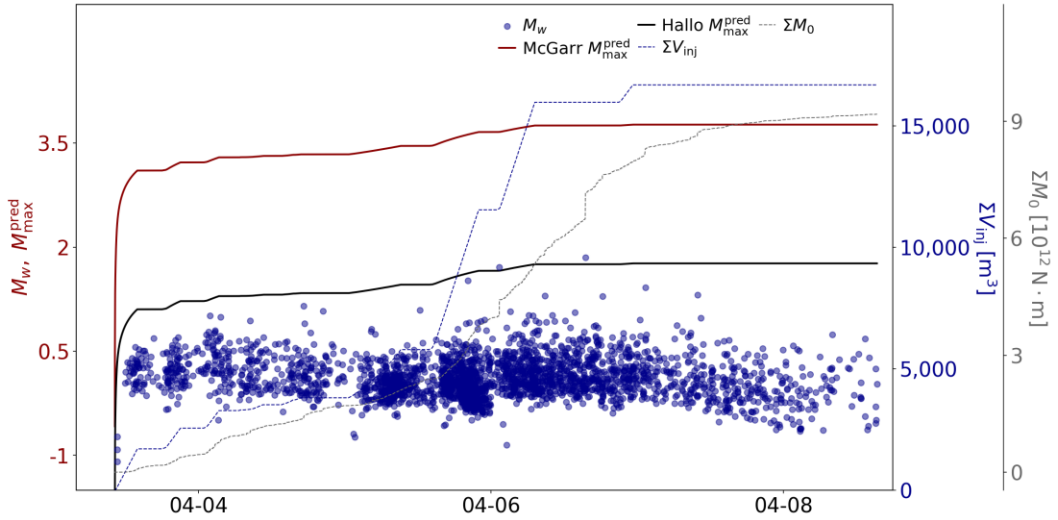

Figure 5: Temporal evolution of observed M_w and predicted M_{max} during the April 2024 Utah FORGE stimulation. Predictions are shown for McGarr's model and Hallo's model, together with cumulative injected volume and cumulative seismic moment.

4.2 PGA and PGV

Figure 4 shows the spatial distribution of predicted ground motions for a seismic event with moment magnitude Mw 1.85 at the Utah FORGE site. Panels A and B present Peak Ground Velocity (PGV) and Peak Ground Acceleration (PGA), respectively. Both PGV and PGA exhibit clear radial decay away from the FORGE injection zone, with the highest ground motion levels concentrated near the source location. Predicted ground motions decrease with increasing distance due to geometric spreading and attenuation, while spatial variations reflect local site effects incorporated through the depth and Vs30 information. Nearby communities, including Milford, Minersville, and Beaver, experience substantially lower PGA and PGV levels than in the immediate vicinity of the FORGE site, indicating limited ground-motion impact at these locations for this magnitude scenario.

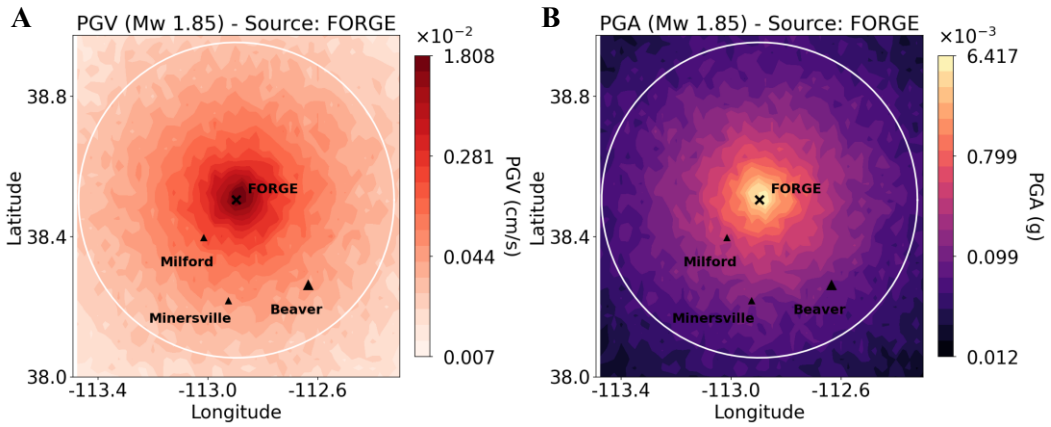

Figure 6: Spatial distribution of predicted ground motions for a M_w 1.85 seismic event at the Utah FORGE site. (A) Peak Ground Velocity (PGV, cm/s) and (B) Peak Ground Acceleration (PGA, g).

4.3 Comparison

To evaluate the operational implications of the predicted M_{max}, Figures 7 and 8 present PGV and PGA estimates at four representative locations: the Utah FORGE site, Beaver, Milford, and Minersville. Ground motions were computed using the observed M_{max} as well as the predicted M_{max} values from McGarr's and Hallo's models. It can be observed that the PGV and PGA corresponding to the observed magnitudes(April 2022, M_{max} = 0.52, and April 2024 M_{max} =1.85) remain well below human perception thresholds (PGV < 0.1 cm/s and PGA < 0.001 g) (Wald et al., 1999).

Hallo's model predicts an M_{max} of 1.1 for the April 2022 stimulation, slightly higher than the observed value, and an M_{max} of 1.8 for the April 2024 stimulation, slightly lower than the observed value. In both cases, the resulting PGV and PGA estimates remain below human perception thresholds at all evaluated locations. In contrast, McGarr's model yields substantially larger M_{max} values (3.1 for April 2022 and 3.8 for April 2024), leading to predicted PGV and PGA levels that exceed perception thresholds. However, no perceptible ground motion was reported at the Utah FORGE site or surrounding communities, including Beaver, Milford, and Minersville, during either stimulation phase. This discrepancy indicates that McGarr's model represents a conservative upper bound on M_{max} for this site and may substantially overestimate the realized seismic hazard.

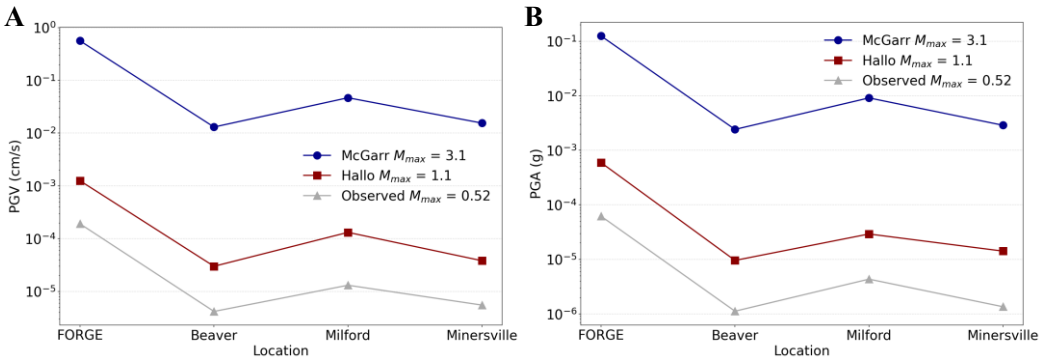

Figure 7: Comparison of PGV and PGA derived from observed and model-predicted M_{max} values for the April 2022 Utah FORGE stimulation.

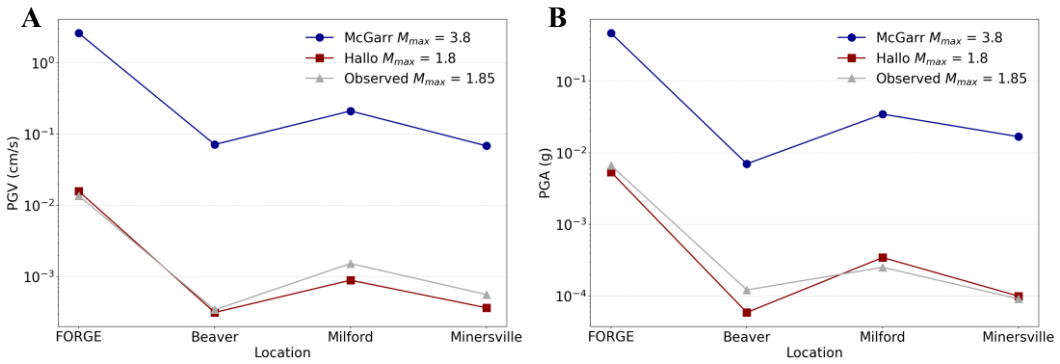

Figure 8: Comparison of PGV and PGA derived from observed and model-predicted M_{max} values for the April 2024 Utah FORGE stimulation.

5. CONCLUSIONS

This study presents an integrated framework that combines M_{max} and ground-motion predictions to support real-time seismic hazard assessment during enhanced geothermal system operations at the Utah FORGE site. By linking source-level M_{max} estimates to site-specific PGA and PGV predictions, the approach enables a direct and quantitative evaluation of potential operational impacts under evolving injection conditions.

The M_{max} predictions obtained using McGarr's and Hallo's methods were different, that reflect their underlying assumptions. McGarr's volume-based method produces conservative upper-bound estimates of M_{max} that substantially exceed the observed maximum magnitudes during both the April 2022 and April 2024 stimulations. In contrast, Hallo's seismic-moment-based method yields lower M_{max} estimates that are more consistent with the observed seismicity, providing a closer representation of the realized earthquake-size distribution at Utah FORGE.

As illustrated in Figures 7 and 8, ground motions predicted using the observed M_{max} and Hallo-based M_{max} remain below commonly cited human perception thresholds for both PGA and PGV at all evaluated locations. Conversely, ground motions associated with the McGarr-based M_{max} exceed perception thresholds despite the absence of reported felt events. This comparison demonstrates that integrating GMPE-derived ground motion estimates with M_{max} predictions enables evaluation of whether predicted source magnitudes are overly conservative relative to observed impacts.

Overall, the integrated M_{max}–GMPE framework provides a robust and transparent way to translate seismic source forecasts into actionable ground-motion metrics. This capability is valuable for informing traffic-light protocols and operational decision-making in geothermal stimulation projects, providing a data-driven basis for risk mitigation while explicitly accounting for uncertainty in induced seismicity.

ACKNOWLEDGEMENT

This project was supported by the Utah FORGE initiative, sponsored by the U.S. Department of Energy, under the project titled "Cutting-edge application of machine learning, geomechanics, and seismology for real-time decision-making tools during stimulation". We also thank Ryan Schultz for his valuable insights on M_{max} predictions and their application to induced seismicity monitoring.

REFERENCES

Atkinson, G. M. (2015). Ground-Motion Prediction Equation for Small-to-Moderate Events at Short Hypocentral Distances, with Application to Induced-Seismicity Hazards. *Bulletin of the Seismological Society of America*, *105*(2A), 981–992. https://doi.org/10.1785/0120140142

Atkinson, G. M., & Boore, D. M. (2006). Earthquake Ground-Motion Prediction Equations for Eastern North America. *Bulletin of the Seismological Society of America*, *96*(6), 2181–2205. https://doi.org/10.1785/0120050245

Bommer, J. J., Douglas, J., Scherbaum, F., Cotton, F., Bungum, H., & Fäh, D. (2010). On the Selection of Ground-Motion Prediction Equations for Seismic Hazard Analysis. *Seismological Research Letters*, *81*(5), 783–793. https://doi.org/10.1785/gssrl.81.5.783

Castellaro, S., Mulargia, F., & Rossi, P. L. (2008). Vs30: Proxy for Seismic Amplification? *Seismological Research Letters*, *79*(4), 540–543. https://doi.org/10.1785/gssrl.79.4.540

Chase, R. E., Liel, A. B., Luco, N., & Baird, B. W. (2019). Seismic loss and damage in light-frame wood buildings from sequences of induced earthquakes. *Earthquake Engineering & Structural Dynamics*, *48*(12), 1365–1383. https://doi.org/https://doi.org/10.1002/eqe.3189

Dyer, B. (2022). Utah FORGE: Updated Seismic Event Catalogue from the April, 2022 Stimulation of Well 16A(78)-32. (D. Karvounis,

Ed.). University of Utah Seismograph Stations. https://doi.org/10.15121/1908927

Dyer, B., Karvounis, D., Meier, P., Fiori, R., & Jaques, P. (2024). Utah FORGE: GES Well 16A(78)-32 and Well 16B(78)-32 Stimulation Seismic Event Catalogs. University of Utah Seismograph Stations. https://doi.org/10.15121/2455012

Ellsworth, W. L. (2013). Injection-Induced Earthquakes. *Science*, *341*(6142), 1225942. https://doi.org/10.1126/science.1225942

Ellsworth, W. L., Giardini, D., Townend, J., Ge, S., & Shimamoto, T. (2019). Triggering of the Pohang, Korea, Earthquake (Mw 5.5) by Enhanced Geothermal System Stimulation. *Seismological Research Letters*, *90*(5), 1844–1858. https://doi.org/10.1785/0220190102

van der Elst, N. J., Page, M. T., Weiser, D. A., Goebel, T. H. W., & Hosseini, S. M. (2016). Induced earthquake magnitudes are as large as (statistically) expected. *Journal of Geophysical Research: Solid Earth*, *121*(6), 4575–4590. https://doi.org/https://doi.org/10.1002/2016JB012818

England, K. (2024). Utah FORGE: Wells 16A(78)-32 and 16B(78)-32 Stimulation Pressure and Circulation Data April, 2024. Energy and Geoscience Institute at the University of Utah. https://doi.org/10.15121/2371032

Gutenberg, B., & Richter, C. F. (1944). Frequency of earthquakes in California. *Bulletin of the Seismological Society of America*, *34*(4), 185–188.

Hallo, M., Eisner, L., & Ali, M. Y. (2012). Expected level of seismic activity caused by volumetric changes. *First Break*, *30*(7).

Hallo, M., Oprsal, I., Eisner, L., & Ali, M. Y. (2014). Prediction of magnitude of the largest potentially induced seismic event. *Journal of Seismology*, *18*(3), 421–431. https://doi.org/10.1007/s10950-014-9417-4

Li, Z., Eaton, D., & Davidsen, J. (2022). Short-term forecasting of Mmax during hydraulic fracturing. *Scientific Reports*, *12*(1), 12509. https://doi.org/10.1038/s41598-022-15365-6

Mahani, A. B., & Kao, H. (2017). Ground Motion from M 1.5 to 3.8 Induced Earthquakes at Hypocentral Distance < 45 km in the Montney Play of Northeast British Columbia, Canada. *Seismological Research Letters*, *89*(1), 22–34. https://doi.org/10.1785/0220170119

Majer, E. L., Baria, R., Stark, M., Oates, S., Bommer, J., Smith, B., & Asanuma, H. (2007). Induced seismicity associated with Enhanced Geothermal Systems. *Geothermics*, *36*(3), 185–222. https://doi.org/https://doi.org/10.1016/j.geothermics.2007.03.003

McGarr, A. (2014). Maximum magnitude earthquakes induced by fluid injection. *Journal of Geophysical Research: Solid Earth*, *119*(2), 1008–1019. https://doi.org/https://doi.org/10.1002/2013JB010597

McLennan, J. (2022). Utah FORGE: Well 16A(78)-32 Stimulation Data (April, 2022). Energy and Geoscience Institute at the University of Utah. https://doi.org/10.15121/1871203

Niemz, P., McLennan, J., Pankow, K. L., Rutledge, J., & England, K. (2024). Circulation experiments at Utah FORGE: Near-surface seismic monitoring reveals fracture growth after shut-in. *Geothermics*, *119*, 102947. https://doi.org/https://doi.org/10.1016/j.geothermics.2024.102947

Schultz, Ryan, Quitoriano, Vince, Wald, David J, & Beroza, Gregory C. (2021). Quantifying nuisance ground motion thresholds for induced earthquakes. *Earthquake Spectra*, *37*(2), 789–802. https://doi.org/10.1177/8755293020988025

Schultz, R., Beroza, G. C., & Ellsworth, W. L. (2021). A Strategy for Choosing Red-Light Thresholds to Manage Hydraulic Fracturing Induced Seismicity in North America. *Journal of Geophysical Research: Solid Earth*, *126*(12), e2021JB022340. https://doi.org/https://doi.org/10.1029/2021JB022340

Shapiro, S. A., Dinske, C., Langenbruch, C., & Wenzel, F. (2010). Seismogenic index and magnitude probability of earthquakes induced during reservoir fluid stimulations. *The Leading Edge*, *29*(3), 304–309. https://doi.org/10.1190/1.3353727

Wald, D. J., Quitoriano, V., Heaton, T. H., & Kanamori, H. (1999). Relationships between Peak Ground Acceleration, Peak Ground Velocity, and Modified Mercalli Intensity in California. *Earthquake Spectra*, *15*(3), 557–564. https://doi.org/10.1193/1.1586058

Zhang, X., Zhu, W., Salvage, R. O., & Dvory, N. Z. (2025). Deep Neural Network-Based Workflow for Accurate Seismic Catalog Generation from Low Resolution Seismic Data in Enhanced Geothermal System Operations. In *PROCEEDINGS, 50th Workshop on Geothermal Reservoir Engineering*. Stanford University.

Zhang, X., Shimony, E., Wygodny, U., Lellouch, A., & Dvory, N. Z. (2026). Fault Identification Using Multiple Event Catalogs from the Stimulation Operation at the Utah FORGE Site. In *60th U.S. Rock Mechanics/Geomechanics Symposium*. Tucson, Arizona, USA.

Zhang, X., Shimony, E., Song, J., Wygodny, U., Zhu, W., Lellouch, A., & Dvory, N. Z. (2026). Microseismic Location in EGS:

Comparing picking-based and source-imaging workflows on downhole DAS data. In *PROCEEDINGS, 51st Workshop on Geothermal Reservoir Engineering*. Stanford University.

Zhang, X. M., & Dvory, N. Z. (2025) Estimating Fault Slip Potential with CNN-Based Deep Learning: Integrating Mohr-Coulomb and Non-Linear Failure Criteria for Advanced Seismic Risk Assessment. *59th U.S. Rock Mechanics/Geomechanics Symposium*. https://doi.org/10.56952/ARMA-2025-0408